Researchers Journal of Science and Technology (REJOST)
https://rejost.com.ng

Low Pressure-induced Phase Transition Study of α-AlH_3 and its Hydrogen Storage Evaluation for Energy Applications via Electronic, Structural, Thermodynamic and Optical Analysis

A. O. Akpan, S. A. Ekong[¥], J. B. Emah

Abstract

Metal hydrides are currently one of the most investigated materials for energy storage applications. In this study, the structural, electronic, and optical properties of α-AlH_3 have been investigated from density functional theory (DFT) calculations. This work is aimed at studying the low pressure-induced phase transition of α-AlH_3 hydride material in the range of 1 - 8 GPa pressure. Self-consistent field (scf) calculations based on the DFT approach were performed using exchange-correlation functionals from generalized gradient approximation (GGA). Structural properties such as lattice constant (4.6973 Å), formation enthalpy, bond distance of Al – H, Al – Al, and H – H, are observed to be consistent with experiments. The electronic density of state (DOS) revealed the band gap as 2.16 eV. Analysis of the gravimetric storage and volumetric storage capacities, as well as the desorption temperature of α-AlH_3 have been performed. The electronic band structure analysis from increased applied pressures shows that the compound is an indirect band gap semiconductor, and retains this nature via the entire applied pressure. Also, a monoclinic distortion of the compound due to the octahedral [AlH_6] tilting of the unit cell is sustained within the pressure range in this study, and this confirms reported experiments. However, the applied pressure evaluation of the electronic band structure revealed a transition state at 3 GPa. This observation was further confirmed by structural analysis owing to the formation of bonds, with no discontinuity found in the structure at increased pressures. Meanwhile, thermodynamic analysis depicts a transition state at 3 GPa with the free energy observed to be − 0.04 Ry, entropy $S \approx 2.1 \times 10^{-4}$ Ry/K, and heat capacity C_V is 1.457 x 10^{-4} Ry/K at Dulong–Petti limit. The negative free energy verifies the thermodynamic stability of the hydride. Accordingly, the optical study showed an abrupt frequency discontinuity in the spectra of electron energy loss (EEL) function at exactly 3 GPa. The EEL function profile reveals the hydride as a promising photo-absorber at energies below 33 eV.

✉ S. A. **Ekong**: sylvesterekong@aksu.edu.ng

Department of Physics, Akwa Ibom State University, Ikot Akpaden, Nigeria.

Keywords: Electronic analysis; Hydrogen storage; Phase transition; Optical properties

Article history
Received: July 21, 2025
Received in revised form: September 17, 2025
Accepted for publication: September 20, 2025
Available online: September 22, 2025

1.0 Introduction

Hydrogen has been a subject of study for years as an exciting energy source, but its main challenge lies in large-scale storage. Storing hydrogen in suitable materials has emerged as a potential solution. These materials need to be stable, safe, affordable, recyclable, and capable of releasing hydrogen efficiently (Bencheikh *et al*., 2024; Ekong *et al*., 2014a). Being a subject of classic scientific debates with remarkable technological relevance, metal hydrides have in recent time impacted and revolutionized the global energy economy (Usman *et al*., 2024; Rehman *et al*., 2023). Most energy generated comes from non-renewable fossil fuels. The continuous increase in the world's energy demand requires updated innovative strategies, and research on sustainable energy for storage capacity (Ahmed *et al*., 2024; Tufail *et al*., 2025). Hydrogen storage system is considered one of the most promising energy sources/carriers (Pan, 2024) that has the potential to displace non-renewable petroleum derivatives, with lower carbon-dioxide emissions, eco-friendliness, and sustainability (Rehman *et al*., 2024). Compounds of this family including light metal hydrides and their complexes have been elaborately investigated (Bencheikh *et al*., 2024; Pan *et al*., 2022; Savić *et al*., 2017; Ekong *et al*., 2016; 2015; Song, 2013).

Among binary metal hydrides, aluminum trihydride (AlH_3) attracts great attention because its multifarious structural chemistry including the electronic and bonding states remain an important subject of considerable debate experimentally and theoretically (Takeda *et al*., 2011; Ke *et al*., 2005). AlH_3 is physically and chemically useful in alkali batteries as a reducing agent, polymerization catalysts, and portable fuel cells for small sensors (Vajeeston *et al*., 2011; Humphries *et al*., 2013). The metal hydride also finds robust and unique exciting applications in optoelectronics (Karazhanov *et al*., 2007). Its potential has been applauded for energy storage technology, as energy component in rocket propellants (Tatsumi *et al*., 2012; Vajeeston *et al*., 2008), and as an onboard power source for vehicles (Karazhanov *et al*., 2008). AlH_3 when combined with ammonium dinitramide (ADN), becomes a high-energy material often used in aerospace, explosive, and missile industries (Grew *et al*., 2012). Of the seven polymorphic phases of AlH_3 known, the most thermally stable of them all is the α-AlH_3 structure produced using organometallic method (Turley & Rinn, 1969; Brower *et al*., 1976). The electronic structures of AlH_3 are characterized by Al-H-Al bridges due to the type of [AlH_6] octahedra connection (Drozd *et al*., 2012). As the most stable phase with the highest density (Song, 2013), α-AlH_3 has a trigonal structure (with space group $R\bar{3}c$).

Recently, Pan *et al*. (2022) in a new insight reported the structural and physical properties of α-AlH_3 from first-principles calculations. According to them, AlH_3 hydride is a typical hydrogen storage material due to its high storage and low decomposition temperature, but the structural feature of AlH_3 remains controversial and the optical properties are unclear. Very recently, Bencheikh *et al*. (2024) conducted density functional theory (DFT)-based modeling and simulation of the structural and optoelectronic properties of aluminum trihydride (β-AlH_3) for hydrogen storage. Nevertheless, low-pressure experimental studies of α-AlH_3 have gone ahead of theoretical investigations, since to the best of our knowledge, only the low-pressure first-principle

DFT calculations by Graetz *et al*. (2006), is found in the literature for α-AlH_3. They reported a low pressure up to 7.0 GPa. Moreover, the diffraction pattern did not change within 4.0 GPa of pressure in their conclusion. Earlier study by neutron diffraction (Goncharenko *et al*., 1991) reported a pressure up to 7.2 GPa. They concluded that the anisotropy of compressibility is non-monotonic, but without any change of symmetry of the aluminum matrix. Again, Graetz *et al*., by increasing Bragg peak asymmetry with pressure reported that no pressure-induced first-order structural transitions were observed up to 7.0 GPa, although the bonding remained unchanged. They further suggested a monoclinic distortion of the rhombohedral unit cell due to the tilting of the [AlH_6] octahedral units at very moderate pressures (1 – 7 GPa). However, the exact pressure at which the distortion will occur was not reported. Contrary to Graetz *et al*., Tkacz *et al*. (2008) in a Raman spectroscopy study observed and reported that a slight monoclinic distortion of the structure was observed at 6.0 GPa pressure. Subsequent low-pressure infrared (IR) spectroscopy and X–ray diffraction structural investigations by Ciezak-Jenkins (2011) reported monoclinic distortion of the rhombohedral unit cell, with structural changes documented between 2.0 and 4.0 GPa. From their findings, an abrupt frequency discontinuity was observed in the Al-H bending and Al-H stretching modes, which implies a structural transformation. Additionally, the IR and X–ray results suggested that the monoclinic distortion occurs sluggishly near 2.5 GPa, but the distortion does not result in a phase transition over the entire pressure range.

Thus, the question of structural changes regarding phase transition in α-AlH_3 at low pressure remains open, since considerable ambiguity exists amongst experiments as to the exact transition point in the phase behavior of AlH_3 at pressures below 10 GPa. Following the ambiguity, Goncharenko *et al.* (2008) argued that the structural deviation could be attributed to slight pressure gradients within the diamond anvil cell in the experiments. Consequently, the exact phase transition point at low pressure warrants further examination. This paper is currently motivated by the optical unclearness of the metal hydride, and aims to study the exact transition pressure point of α-AlH_3 at low pressure theoretically. In condensed matter physics, most theoretical studies are performed by using DFT-based simulation packages (Aliabad & Yalcin, 2017; Ekong *et al*., 2014b). In the current paper, we studied the electronic, thermodynamic and optical phase transition of α-AlH_3 at pressures 1 – 8 GPa based on DFT simulation techniques. We further explored the α-AlH_3 by analyzing physical and structural properties like formation enthalpy, cohesive energy, gravimetric storage and volumetric capacities, desorption temperature, bulk modulus, etc. The obtained optimized values are in good agreement with the experiments for the hydride compound. In our results, the Al–H bonding nature remained predominantly covalent within the applied external low pressures, confirming the only DFT report by Graetz *et al*. (2006). Lastly, all the thermal and optical parameters calculated showcased discontinuity at 3 GPa, hence illustrating the same transition point for the compound.

2.0 Computational Procedure

In this study, all calculations are performed utilizing the Quantum Espresso code (Giannozzi *et al*., 2017; 2009) based on DFT, density-functional perturbation theory (DFPT), and quasi-harmonic approximations (QHA) (Baroni *et al*., 2010). The exchange-correlation function was treated within generalized gradient approximation (GGA) with Perdew-Burke-Ernzerhof (PBE) parameterization (Perdew *et al*., 1996). The kinetic energy cutoff is set to 190 Ry, while a reciprocal space sampling (Brillouin zone) of 12 x 12 x 12 k-points grid (Monkhorst & Pack, 1976), with the threshold set to 10^{-10} Ry was used for the α-AlH_3 geometry optimization.

For an accurate description of the electron-ion interactions, the norm-conserving pseudo-potential (NCPP) approach was adopted (Goedecker & Teter, 1996; Hartwigsen *et al*., 1998). To perform the self-consistent field (SCF) calculations at different lattice constants, all structural optimization calculations were carried out using the Broyden–Fletcher–Goldfarb–Shanno (BFGS) minimization algorithm. Other convergence criteria for the ionic minimization were 2.0×10^{-6} Ry for total energy, 1.0×10^{-3} Ry for maximum force, and 0.005 Ry for smearing width to handle the Fermi surface (Malica & Corso, 2020).

Further, to obtain a smooth and better density of state (DOS), a tetrahedra method with an increased k-points grid of 16 x 16 x16 was found suitable for the calculations. Fitting the energy-volume (E–V) data sets to Birch-Murnaghan equation of state (EoS) given in equation (1) using ev.x tool in Quantum Espresso suit, we determine the equilibrium lattice constant and calculated other ground-state parameters (Murnaghan, 1944; Jolayemi *et al*., 2020):

$$E = E_0 + \frac{B_0}{B_0'}(V - V_0)\frac{B_0 V_0}{B_0'(1-B_0')}\left[\left(\frac{V}{V_0}\right)^{1-B_0'} - 1\right] \quad (1)$$

Here, E_0 is the minimum energy, equilibrium volume (V_0), B_0 is the bulk modulus, B_0' is first pressure derivative of B_0. The thermodynamic and optical response properties to photon were computed via QHA and DFPT approaches, as implemented in thermo_pw code (Malica & Corso, 2020)., an extension of Quantum Espresso. The effect of applied pressure as well as temperature for the mentioned properties are given in section 3.3 herein.

3.0 Results and Discussions

3.1 Analysis of Structural Stability and Electronic Properties

Aluminum trihydride (with α-AlH_3 phase) has a trigonal crystal symmetry with $R\bar{3}c$ space group, and a rhombohedral primitive unit cell structure. Showcased in Figure 1, the Al^{3+} atom shared six neighboring equivalent H^{1-} atoms to form AlH_6 octahedra. The corner-sharing octahedral tilt angles are 56.52°. The rhombohedral structure demonstrates the spatial distribution of atoms within the unit cell of α-AlH_3, offering a rudimentary understanding of the crystallographic disposition in this phase. The Wyckoff positions proffer precise coordinates for Al- and H-atoms, aiding the circumstantial characterization of the material structure as follows: Al atoms are positioned at (2/3, 1/3, 1/3), while H atoms are positioned at (0.633, 0.633, 0.250) respectively. To calculate the equilibrium lattice constants, the GGA-PBE approach was employed to minimize the total energy of the unit cell. Further, from the structural optimization we determined properties such as the lattice constant a_0, bond distance (or length) of Al–H, Al–Al, and H–H, and bond angle of Al–H–Al as illustrated in Table 1, and our results are in good standing with the experiments and are within the limits of theoretical values. Consequently, the percentage deviation of our calculated values relative to experiments (Takeda *et al*., 2011; Turley & Rinn, 1969) is depicted in Table 1. The obtained Al–H bond distance (1.7151 Å) reveals the bonding nature of α-AlH_3 as covalent, confirming the works of Takeda *et al*. (2011) and Tatsumi *et al.* (2012) respectively. Moreover, to analyze the thermodynamic stability of our α-AlH_3 material, calculations of the cohesive energy ($E_{Coh.}$), and formation enthalpy (ΔH_f) are confirmed utilizing equations (2) and (3) as provided in (Masood *et al*., 2025).

$$E_{Coh.} = \frac{1}{N}\left[E_{Total}(AlH_3) - E_{Total}(Al) - \frac{3}{2}E_{Total}(H_2)\right] \quad (2)$$

Here $E_{Total}(AlH_3)$ represents the total energy of the hydride, while $E_{Total}(Al)$ and $E_{Total}(H_2)$ the isolated atom energies. A negative cohesive energy value in a material is considered energetically stable.

The formation enthalpy (ΔH_f) for a compound precisely characterizes the variation in a

compound's total energy and its individual stable state constituent energies. The computation of ΔH_f is obtained from Eq (3):

$$\Delta H_f = E_{Total}(AlH_3) - \left[E_{Total}(Al) + \frac{3}{2} E_{Total}(H_2)\right] \quad (3)$$

where $E_{Total}(AlH_3)$ represents the total energy of α-AlH3 hydride, while $E_{Total}(Al)$ and $E_{Total}(H_2)$ denote the stable individual energies of the Al- and H-atoms. The calculated value for ΔH_f remains negative in all materials, confirming the stability of α-AlH3 in this study as shown in Table 1.

Table 1: Structural properties of bulk α-AlH3 as compared with other studies

Ref.	Methods/ Codes	Lattice constant a_0 (Å)	Al–H Bond-length (Å)	Al–Al Bond-length (Å)	H–H Bond-length (Å)	Al-H-Al Bond angle (°)	$E_{Coh.}$ (eV/fu)	ΔH_f (kJ/mol)
This work	Quantum Espresso code	4.6973 ± 0.17%	1.7151 ± 0.09%	3.2356 ± 0.04%	2.4175 ± 1.65%	141.2130 ± 1.3%	-13.6582	-6.2000
[a]Exp.	X-ray and neutron diffraction	4.6990	1.7150	3.2360	2.4340	141.2000	–	–
[b]Exp.	Neutron diffraction	–	1.7000	–	2.4000	–	–	–
[c]Exp.	X-ray emission and absorption spectroscopy	–	1.7160	–	–	–	–	–
[d]Exp	X-ray diffraction patterns	–	1.7200	3.2400	–	–	–	–
[e]Exp	X-ray diffraction/ thermal analyses	–	–	–	–	–	–	-6.0000
[f]Cal.	Wien2k code	–	1.7174	3.3244	2.4112	–	–	-7.6000

[a]Turley & Rinn, 1969; [b]Goncharenko *et al*., 1991; [c]Takeda *et al*., 2011; [d]Graetz *et al*., 2011; [e]Orimo *et al*., 2006; [f]Savić *et al*., 2017

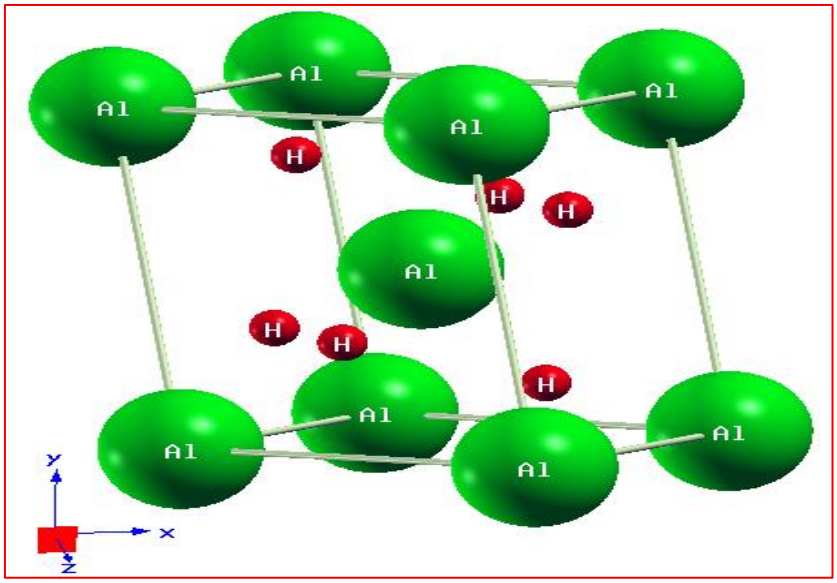

Figure 1: The rhombohedral crystal structure of α-AlH3 for RHL1: α < 90⁰. The large spheres denote Al-atoms while the small spheres denote H-atoms respectively.

Following the realization of geometry optimization at P = 0 GPa, other ground state electronic parameters such as the bulk moduli (B_0), first pressure derivative of B_0 (B_0'), and equilibrium volume (V_0) were successfully determined by fitting the calculated total energy as a function of unit cell volume (E–V data) of the hydride into Birch-Murnaghan equation of state (EoS) given in Eq (1). These characteristic parameters are detailed in Table 2. Herein, it's worth noting that our obtained results though in concord with experiments encompass a sundry range of B_0 reported theoretically. The bulk modulus plays a vital factor in determining the structural stability of materials owing to the resistive ability to deform or crack. In addition, the obtained B_0 value from the EoS fitting agrees well with the results of Baranowski *et al*. (1985) and Graetz *et al*. (2006), whose values were experimentally obtained by fitting their data into Birch EoS and Birch-Murnaghan EoS respectively. Of the two theoretical results by (Graetz *et al*., 2006; Vajeeston *et al*., 2008) reported for B_0, the closest (Graetz *et al*., 2006) has a deviation of 16.5 % and 18.4 % from the experiments. However, this study gives a deviation of 4.4 % and 2.04 % respectively in a similar manner. This is an indication that the calculated value of B_0 in the current study is in good accord with the experiment. The deviation in the B_0 value arising from this study is not unusual to first principles DFT calculations. Thus, the computed bulk modulus (B_0) in this study based on comparison indicates that the α-AlH_3 material is thermodynamically stable due to the high value of B_0 recorded.

Displayed in Figure 2 and Figure 3 are the electronic density of state (DOS) and projected density of states (PDOS) of the compound when no pressure is applied. Evidently, from the DOS and PDOS profiles, the computed energy band gap value (2.16 eV) obtained in this study falls within the limits of theoretical accuracy as given in Table. The predominant contributions of the photon energy to electron momentum in the highest-occupied-molecular-orbital (HOMO) region of the PDOS depicted in Figure 3 is composed of considerably 8(H)1s and 2(Al)2p orbitals which hybridized for transitions to lowest-unoccupied-molecular-orbital (LUMO). The estimated DOS is 3.57 per eV.

3.2 Hydrogen Storage Properties

The study calculates the gravimetric capacity and volumetric capacity of α-AlH_3 hydride for hydrogen storage applications. The gravimetric hydrogen storage capacity for the hydride structure was calculated using Eq. (4) and represented by C_{wt}% in Table 3. Gravimetric capacity measures the quantity of stored hydrogen per unit mass of the hydride compounds (Rehman *et al*., 2024; Shahzad *et al*., 2024):

$$C_{wt}\% = \left(\frac{(^{H}/_{M})\, m_H}{M_{Host} + (^{H}/_{M})\, m_H}\right) \times 100\% \quad (4)$$

Similarly, the volumetric hydrogen storage capacity ($\beta_{Vol.}$) is expressed as in Eq. (5).

$$\beta_{Vol.} = \frac{N_H\, m_H}{V(L)\, N_A} = \frac{N_H\, m_H}{Vol.(\text{Å})^3} \quad (5)$$

In this expression, m_H and M_{Host} represents the molar mass of H_2 and Al, whereas the H/M is the ratio of hydrogen atoms to metal atoms, and in this case, it is three. The calculated maximum storage capacity of the hydride α-AlH_3 is 10.08 wt.% for gravimetric hydrogen storage capacity and 145.30 kg/m^3 for volumetric hydrogen storage capacity. Our calculated gravimetric and volumetric hydrogen storage values are in better agreement with reported experiments as shown in Table 1, (10.10 wt.% and 149 kg/m^3) (Graetz & Reilly, 2006), indicative of the hydride's suitability for hydrogen storage applications. The current study records satisfying gravimetric storage ratio to experiment, with a slightly lower calculated volumetric hydrogen storage capacity, a behavior of which could be attributed to reduced space available (owing to the slight 0.17% reduction in lattice constant value) within the rhombohedral unit cell for hydrogen to desorb and adsorb easily

Table 2: Electronic properties of α-AlH_3 as compared with other studies

Ref.	Methods/ Codes	Bulk modulus B_0 (GPa)	Pressure derivative B_0'	Equilibrium volume V_0 $(Å^3/\text{f.u.})$	Band gap energy (eV)
This work	Quantum Espresso code	50.00	5.00	33.69	2.16 (GGA)
[a]Exp.	X-ray diffraction	49.00	1.00	–	–
[a]Cal.	CASTEP code	40.00	3.10	–	–
[b]Cal.	VASP code	28.00	5.40	33.50	2.34 (GGA)
[c]Cal.				–	3.54 (GW)
	VASP code	–	–		2.18 (GGA)
					1.79 (LDA)
[d]Cal.	DMol^{3}package	–	–	–	2.53 (GGA)
[e]Cal.	WIEN2K code	–	–	–	2.00 (LDA)
[f]Cal.	Electron energy loss spectroscopy	–	–	–	1.40 (LDA)
[g]Cal.	VASP code	–	–	–	2.20 (GGA)
[h]Cal.	VASP code	–	–	–	2.10 (GGA)
[i]Exp.	X-ray and neutron diffraction	–	–	33.72	–
[j]Exp.	Energy dispersive X-ray	47.90	3.30	–	–
[k]Exp.	Neutron diffraction	38.90	5.00	–	–
[l]Exp.	Raman and X-ray diffraction	45.00	4.00	–	–
[m]Exp.	X-ray diffraction	42.30	3.50	–	–
[n]Exp.	X-ray emission and absorption spectroscopy	–	–	–	3.1

[a]Graetz *et al*., 2006; [b]Vajeeston *et al*., 2008; [c]Van Setten *et al*., 2007; [d]Vajeeston *et al.*, 2011; [e]Aguayo & Singh, 2004; [f]Tatsumi *et al*., 2012; [g]Ke *et al*., 2005; [h]Wang *et al.*, 2008; [i]Turley & Rinn, 1969; [j]Baranowski *et al.*, 1985; [k]Goncharenko *et al.,* 1991; [l]Drozd *et al.,* 2012; [m]Goncharenko *et al.,* 2008; [n]Takeda *et al.*, 2011

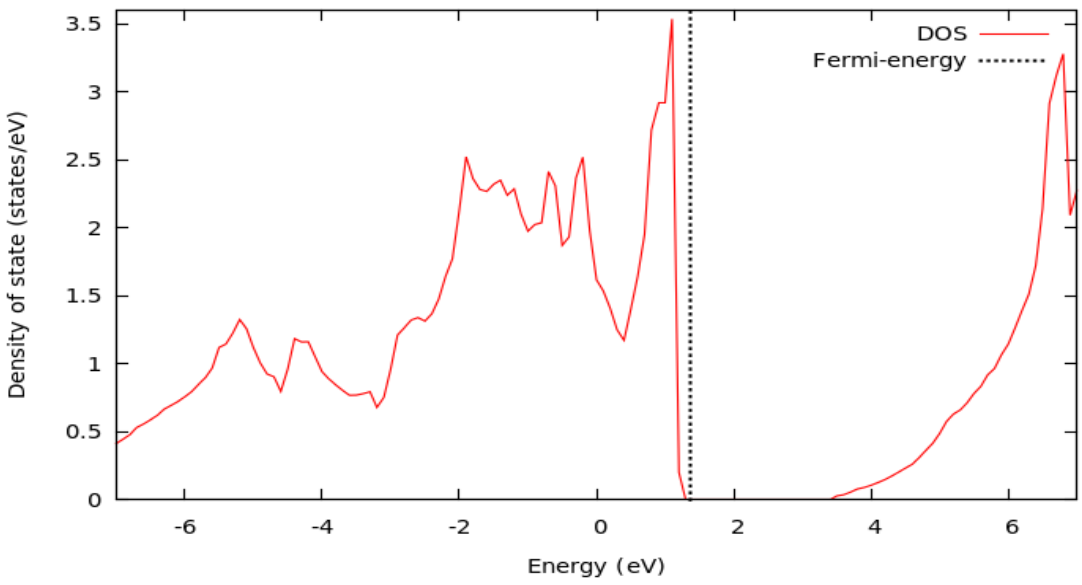

Figure 2: Density of state (DOS) plot as a function of energy for α-AlH_3. The vertical dotted line indicates the Fermi energy level (E_F) position. A band gap energy of 2.16 eV was obtained.

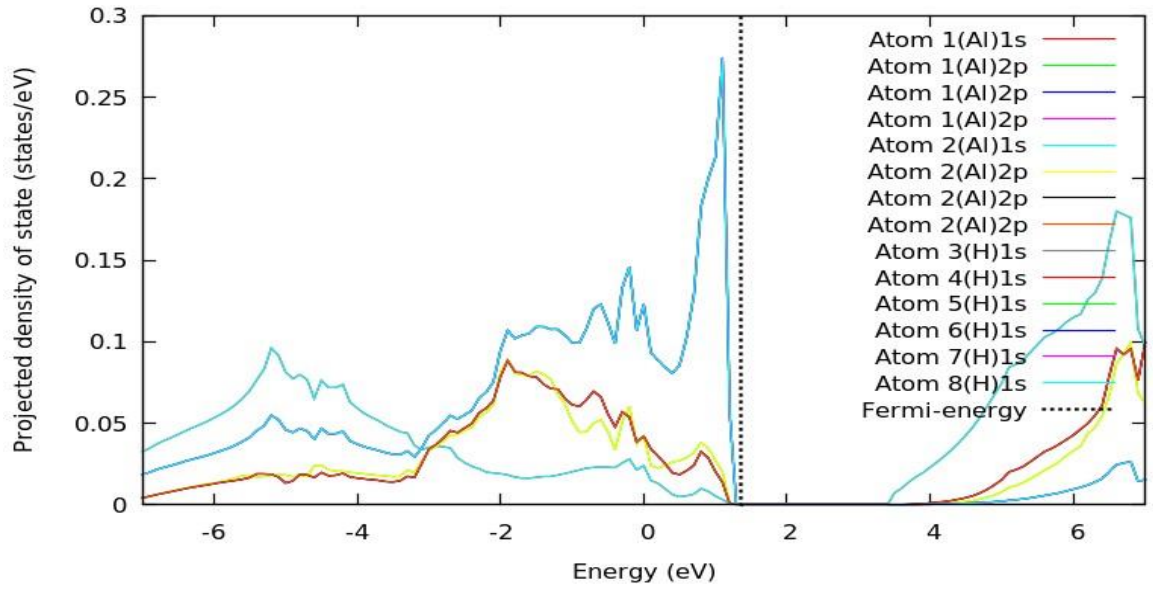

Figure 3: Projected density of states (PDOS) for all s- and p-states in the unit cell of bulk α-AlH_3. The vertical dotted line indicates the Fermi energy level (E_F) position. The obtained band gap is 2.16eV with a bond overlap population of 0.27.

Furthermore, hydrogen desorption temperature (T_{HD}) is the temperature required to release deposited hydrogen within a material (Obeidat *et al*., 2025), and it is estimated as:

$$\Delta G = \Delta H_f - T_{HD} \cdot \Delta S \qquad (6)$$

Here, ΔH_f is the calculated formation enthalpy, and ΔS denotes the entropy change in solids. Indeed, the Gibbs free energy is a significant thermodynamic quantity that finds usefulness in describing the properties of hydrides (Ain *et al*., 2024). The temperature at which the standard Gibbs energy equals zero is referred to as the decomposition temperature. Thus, the desorption temperature for hydrogen is estimated according to Eq. (6) and given in Table 3. The change in entropy of hydrogen at normal conditions is given as: $\Delta S(H_2) \approx \Delta S$ = 130.7 J/mol-K (Obeidat *et al*., 2025). Moreover, it represents the ΔS associated with the transformation of H_2 from a disordered gas to an ordered solid (Graetz & Reilly, 2006). However, the studied hydride exhibits low desorption temperature T_{HD} value in satisfactory agreement with the experiment as depicted in Table 3, making it a promising candidate for hydrogen filling and low-power fuel cell applications.

Table 3: Hydrogen storage properties of α-AlH_3, including the gravimetric hydrogen storage capacity C_{wt}.%, the volumetric hydrogen storage capacity $\beta_{Vol.}$ (gH_2/L), the desorption temperature T_{HD} (K)

α-AlH_3	C_{wt}%	$\beta_{Vol.}$ (gH_2/L)	T_{HD} (K)
This work	10.08	145.30	47.44
Exp.	10.10[(a)]	149.00[(a)], 148.00[(b)]	48.5[(a)], 46.4[(c)]

[(a)]Graetz & Reilly, 2006; [(b)]Graetz *et al*., 2011; [(c)]Sinke *et al*., 1967

3.3 Low Pressure-induced Electronic, Thermal and Structural Transition in α-AlH_3

Unveiling the intricacy and nature of a material's properties under pressure is paramount owing to the decisive role pressure effects can have in sculpting both material's configurations and stability. The electronic and structural properties of α-AlH_3 were computed for various applied

pressures ranging from 1 to 8 GPa as shown in Figure 4. Understanding the characteristics of the α-AlH_3 under low pressures is key to a crucial step in determining and establishing various properties. Depicted in Figure 4(a) are the electronic band structures (EBS) obtained, and Figure 4(b) the projected density of states (PDOS) for different applied pressures (compressive stress). The EBS obtained by applying pressures retained its typical indirect band gap semiconducting nature, while still sustaining the LUMO position of the highly symmetrical Γ-point. Further, with the increasing compressive stress, the bottom of the LUMO continually moves towards high energy as revealed in Figure 4(a) from 1 GPa to 7 GPa while the top of the HOMO remains unchanged. This movement toward higher energy is linked to compressive strain-dependent effects, yielding increasing Fermi-energy levels (see Figure 8). Consequently, in Figure 4(a), a gradual disappearance of a single-band was observed at the top LUMO region between the Z–B|B_1 symmetry positions up to 3 GPa respectively.

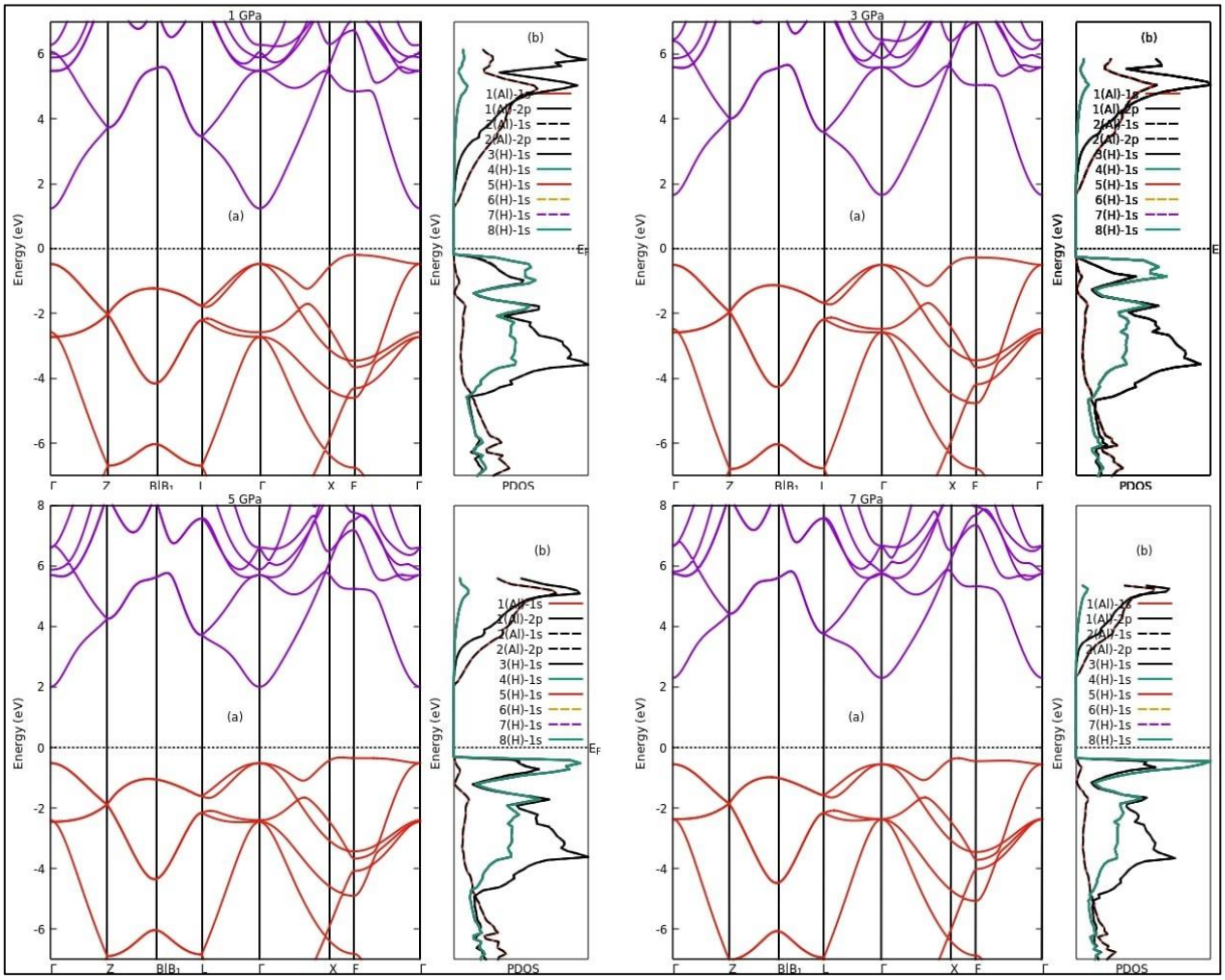

Figure 4: (a) Electronic band structure and (b) Projected density of states (PDOS) along high symmetry Brillouin zone directions for 1 GPa, 3 GPa, 5 GPa, and 7 GPa respectively. The horizontal dotted black-line indicates the position of the Fermi Energy Level (E_F).

Likewise, the minimum LUMO band at 1 GPa goes far below the 2.0 eV at first. With the observed gradual upward increase in minimum LUMO to higher energies, this upward trend continues even above 2.0 eV as the applied pressure approaches 8 GPa. Moreover, from 3 GPa to 4 GPa, the single-band disappeared completely, and thereafter, from 5 GPa the reappearance of the single-band is again noticed

with increasing downward shoot or movement. This behavior is sustained for the rest of the higher pressures with corresponding energy increment in the positive direction of the vertical energy profile. Confirmed in Figure 7 is the characteristic energy increment of the band gap energy by the DOS (density of state) profile.

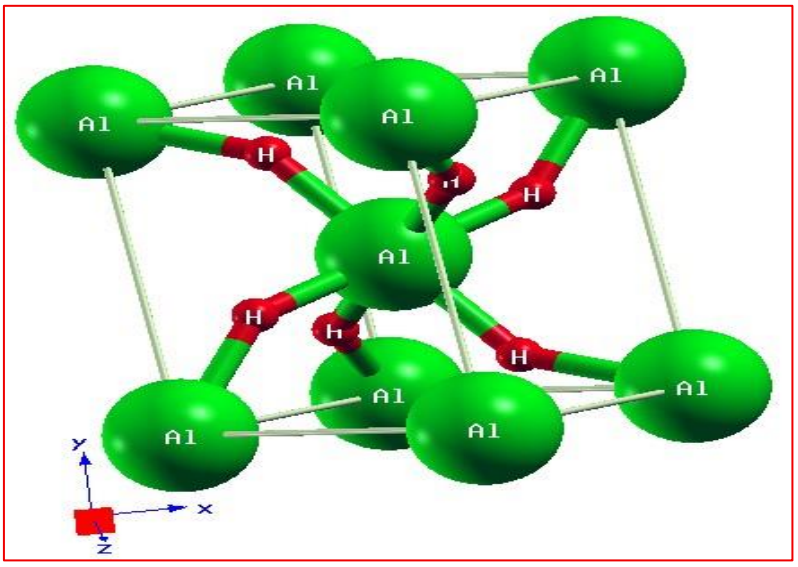

Figure 5: Structural phase transition of α-AlH_3 due to pressure at 3 GPa (with x-, y-, z-coordinates)

Notably, this increment in the energy profile shows the transfer of electron momentum from the HOMO to LUMO regions due to excitations resulting from compression. Additionally, the behavior of the compound to exhibit a disappearance and reappearance of single-band is a characteristic of reconstructive transitions (Mujica *et al*., 2003) resulting from solid-solid phase transitions driven by pressure changes, which in our case shows exactly where the transition starts. Furthermore, at 3 GPa the formation of new bonds was found in the crystal structure as depicted in Figure 5. It was therefore observed to have been sustained at applied pressures up to 8 GPa, hence showing the stability of the material structure within the prescribed pressure range.

A material's total heat content is termed enthalpy (H), often representing the heat absorbed (endothermic) or released (exothermic) during a process. Nevertheless, a negative enthalpy change ($\Delta H < 0$) showcases the exothermic nature of a material that yields bond formations, whereas a positive enthalpy change ($\Delta H > 0$) showcases endothermic nature resulting in bond breaking (Ren *et al.,* 2023; Yu & Liu, 2025). Figure 6(a) illustrates the change in enthalpy in kJ/mol. for α-AlH_3 at varying low pressures. The obtained negative ΔH values are indications leading to forming new, stable bonds in α-AlH_3 with lowering potential energy, and a release of excess energy. The result provides insight into the thermodynamic favorability of the hydride by quantifying the energy released. From the Figure, an equilibrium is attained starting from 3 GPa. Consequently, the propensity of the hydride suggests the stability and start of bond formation at 3 GPa pressure. This again confirms the electronic and structural transition results of Figures 4 and 5, respectively. The illustrations in Figures 6(b) – (d) showcase the temperature dependence of free energy, entropy, *S*, and constant volume heat capacity C_V at different pressures in the temperature range 0–800 K. In Figure 6(b), the free energy has its minimum value at 3 GPa observed to be − 0.04 Ry for the material. The negative free energy verifies the thermodynamic stability of the hydride. Clearly, within the pressure range, it

can be seen in Figure 6(b) that the free energy at 3 GPa, showcase the most stable equilibrium transition state for the studied hydride. The more negative a free energy is the higher the entropy (Musari, 2021). This analysis depicts a more negative free energy value, −0.04 Ry, at 3 GPa, and displayed a lesser negative value at higher pressures. This behavior at 3 GPa supports the observed electronic transition state in Figure 4. Displayed in Figure 6(c) is the entropy (*S*) plot of α-AlH_3 for various pressures. Entropy, reflects the thermal energy of a material. The rise in temperature at fixed pressure can be seen resulting to a rise in entropy *S*. The *S* value in Figure 6(c) rises upward until 3 GPa, and thereafter reduces to the minimum. The increase in *S* is a consequence of the thermal excitation of electrons. As a result, electrons acquire higher energy and transit to higher energy states at a fixed pressure. From Figure 6(c) the highest entropy value is $S \approx 2.1 \times 10^{-4}$ Ry/K at 3 GPa pressure. This is in concord to the analysis of the free energy. Thus, the exhibited discontinuity in the uprise of *S* could be attributed to the phase transition at the same pressure as in Figures 4 and 5, respectively.

The specific heat capacity C_V in Figure 6(d) increases exponentially with temperature due to the increase in thermal excitation of electrons within the hydride. Similar to the *S* plot of Figure 6(c), the C_V plot confirms the assertion at 3 GPa for the hydride, as the highest spectra falls within the same pressure peak.

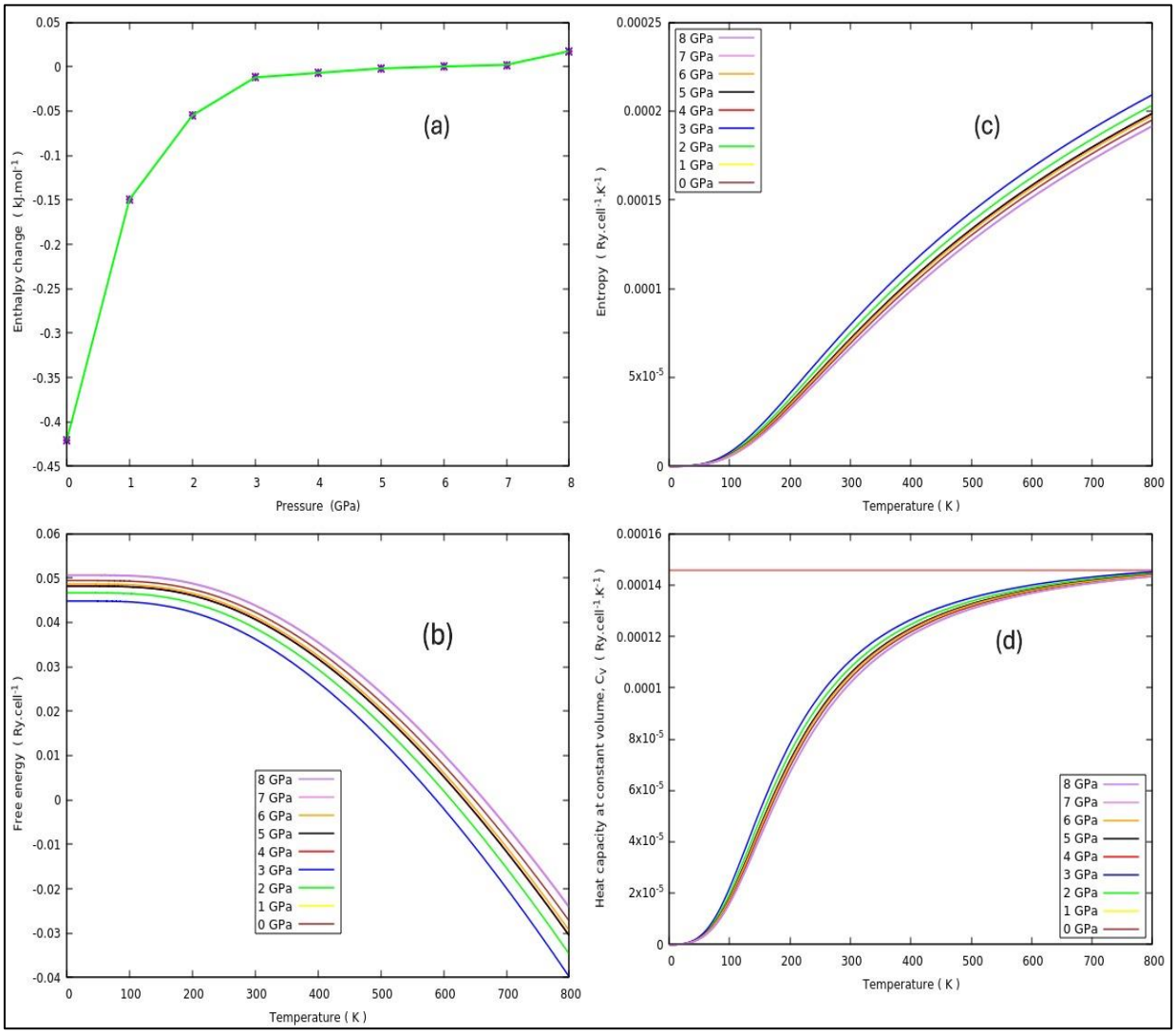

Figure 6: Enthalpy change vs pressure (a), Free energy (b), Entropy (c) and Heat capacity (d) as functions of temperature

The concept of Debye temperature T_D is fundamental as it links many physical parameters, as well as describing the C_V behavior. We observe in Figure 6(d) that the isochoric C_V of the α-AlH_3 increases exponentially with temperature for T < 450 K. For temperatures much higher than the Debye temperature ($T > T_D$), the C_V approaches the Dulong and Petit law (Mouchou *et al*., 2023) as indicated with upper red line in Figure 6(d). From our result, one can see that at T > 500 K, all phonon modes at higher temperatures are sufficiently excited by thermal energy. The C_V reflects the heat storage capacity of a material and in this study, the recorded maximum value of C_V = 0.1457 mRy/cell/K (i.e. 191.35 J/mol.) at 3 GPa was obtained.

Nevertheless, it is well known that the nature of the band gap is another important property of materials. Most materials are associated with direct band gap due to direct photon emission by electrons, but for indirect band gap, the photons cannot be directly emitted by electrons except by passing through an intermediate state and transferring momentum to the crystal lattice. In the current study, irrespective of the shift in symmetry, all the EBS profiles (see Figure 4(a)) revealed an indirect band gap, and the corresponding eigenvalues are calculated from the DOS as illustrated in Figure 7.

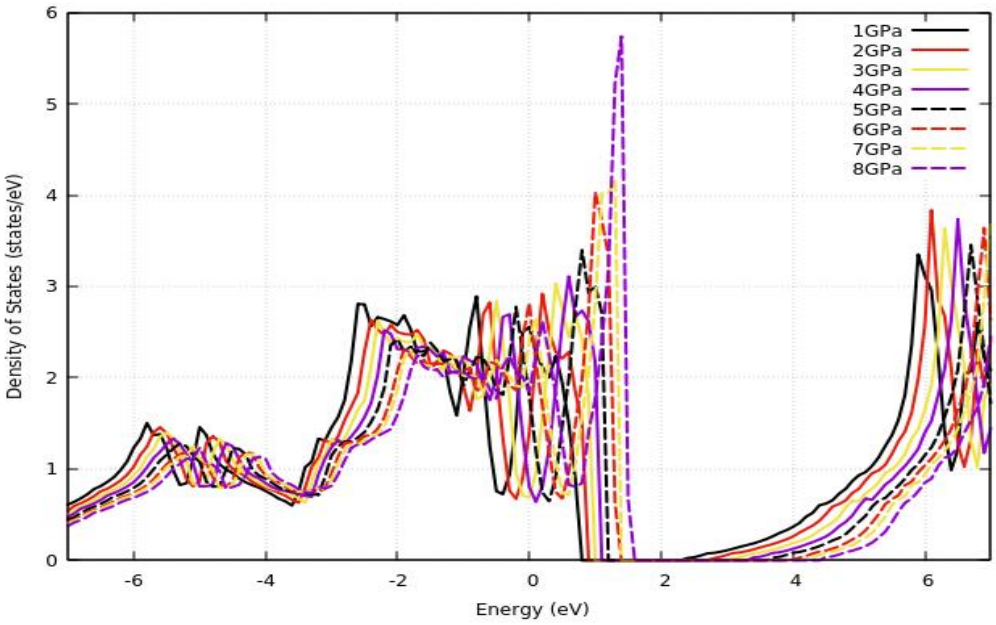

Figure 7: Density of states (DOS) versus energy for the various pressures

The DOS plot shows an increasing band gap nature due to the compressive strain effect arising from reduced unit cell volume influenced by applied pressures. Again, the energy band gap was observed to have increased from 1.423 eV to 2.752 eV within the pressure range of 1 GPa to 8 GPa presented in Figure 7. This increasing trend of band gap value in the DOS plots is similar to that reported by Graetz *et al*. (2006) at moderate pressure. Generally, Fermi energy exhibits increasing characteristics with increasing pressures as confirmed in Figure 8. Shown in Figure 9, Figure 10, and Figure 11 are the pressure-dependent plots of the Al-H-Al bond angle, Al-H bond distance, and volume compression respectively as functions of increasing applied pressure. Consequently, the three Figures exhibit the usual decreasing trend relating to increasing applied pressures. In agreement with the report of Graetz *et al*., the decreasing nature of Figure 10 exhibits a behavior towards strong covalency due to decreasing Al–H bond length resulting from increased applied pressure.

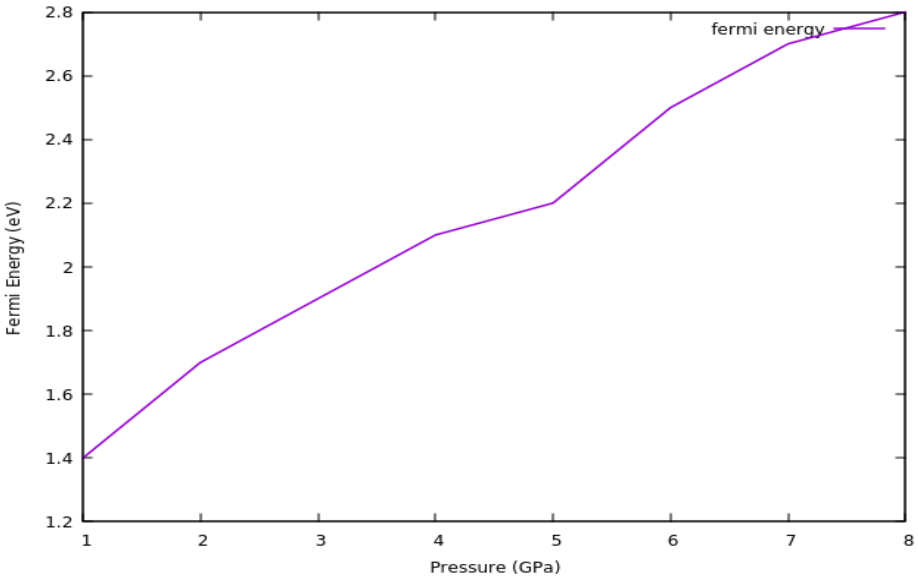

Figure 8: Fermi energy as a function of applied pressure

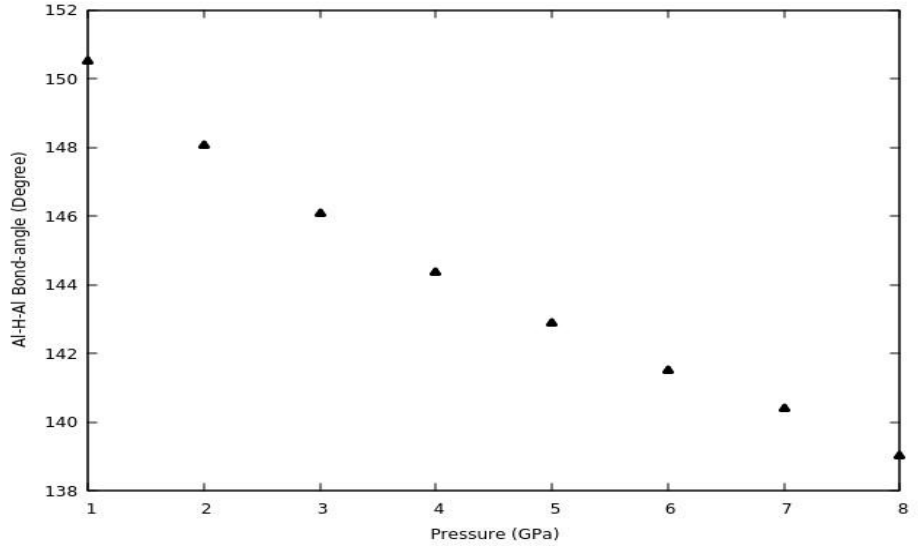

Figure 9: Bond angle as a function of applied pressure

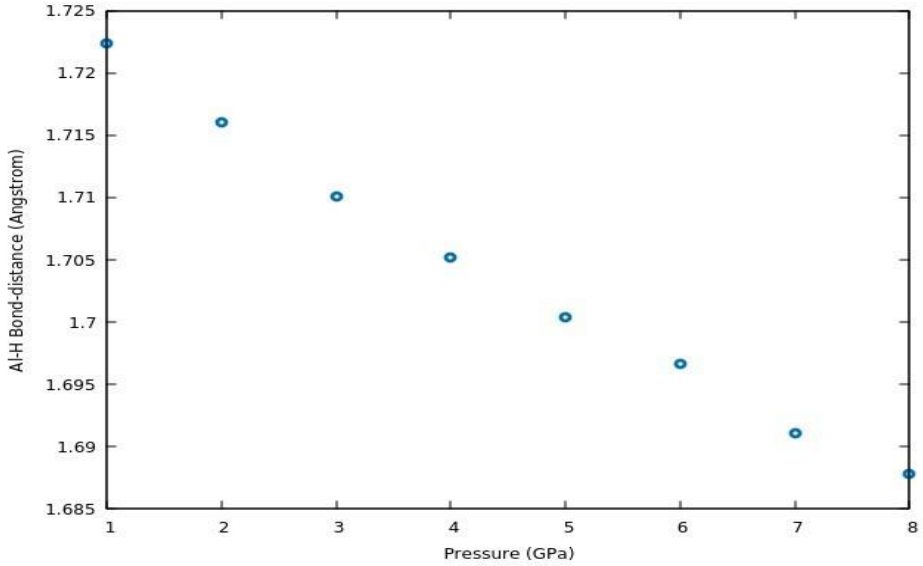

Figure 10: Bond distance as a function of applied pressure

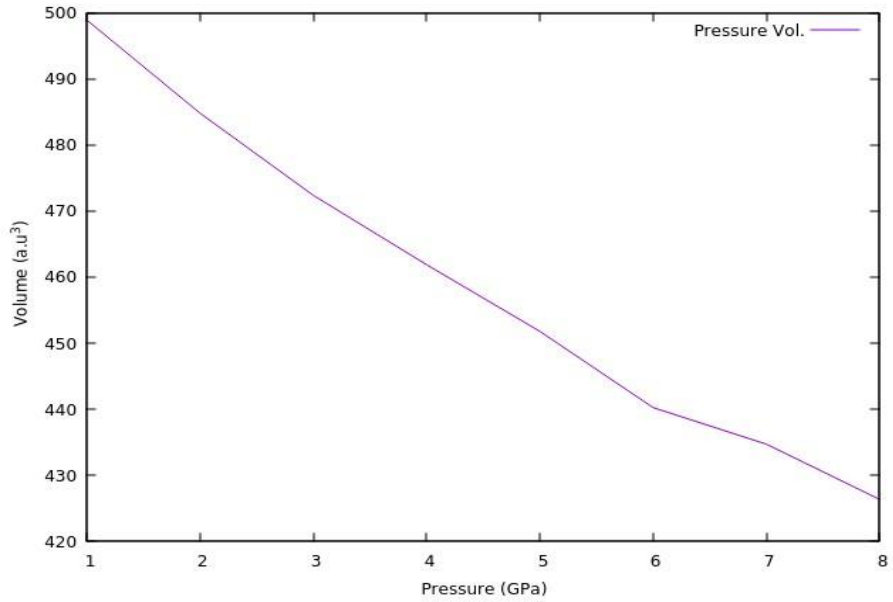

Figure 11: Volume compression at varying applied pressures

3.4 Low Pressure-induced Optical Transition in α-AlH$_3$

In the linear range, the optical response functions of semiconductors to analyze the optical behavior are essential for understanding how they respond to incident photons. The complex dielectric function from the Ehrenreich-Cohen formula (Shahzad *et al.*, 2024) is given by $\varepsilon(\omega) = \varepsilon_1(\omega) + i\varepsilon_2(\omega)$, and quantifies how materials respond to electromagnetic (EM) radiation due to the interaction of photons with electrons (Aliabad & Yalcin 2017) over varying frequencies (ω). The optical properties are measured after the calculations of real $[\varepsilon_1(\omega)]$ and imaginary $[\varepsilon_2(\omega)]$ components of the complex function $\varepsilon(\omega)$. Also, while the polarization is indicated by $\varepsilon_1(\omega)$, the energy dissipation of the system is delineated by (ε_2). Specific equations that relate the components are (Hosen *et al.*, 2025, Ekwere *et al.*, 2024):

$$\varepsilon_1(\omega) = 1 + \frac{2}{\pi} P \int_0^{\infty} \frac{\omega' \varepsilon_2(\omega')}{(\omega')^2 - \omega^2} d\omega' \quad (7)$$

where the momentum operator P is the Cauchy integral. The interband transitions from the EBS yields,

$$\varepsilon_2(\omega) = \frac{1}{\pi}\left[\frac{4\pi e}{m\omega}\right]^2 \sum_{ij} \cdot \int_{BZ}^{\infty} [M_{ij}(k)]^2 \; f_i(1 - f_j) \times \delta[E_f - E_i - \omega] d^3(k) \quad (8)$$

where 'i' and 'j' represent the HOMO and LUMO bands in basis sets and $M_{ij}(k)$ denote the dipole matrix in ij directions. In compliance with the Kramers–Kronig relationship and the direct transition probability between $\varepsilon_1(\omega)$ and $\varepsilon_2(\omega)$, the electron energy loss (EEL) function $L(\omega)$ is computed as:

$$L(\omega) = \mathrm{Im}\left[\frac{-1}{\varepsilon(\omega)}\right] = \frac{\varepsilon_2(\omega)}{\varepsilon_1^2(\omega) + \varepsilon_2^2(\omega)} \quad (9)$$

As a valuable tool for investigating materials' optical response, the function $L(\omega)$ is constituted by plasmon excitations. The optical spectra of Figure 12, and Figure 13 are the obtained results of our dielectric function calculations using equations ((7) – (9)) at different applied pressures of 1 GPa – 8 GPa within the energy spectrum of 0–15 eV. The real dielectric function $\varepsilon_1(\omega)$ of α-AlH$_3$ within the given pressures showed a quick rise to maximum peaks and sharp drops in the low-energy range, as depicted in Figure 12(a). The maximum peak reached by $\varepsilon_1(\omega)$ is 205.21 at 0.25 eV (at 1 GPa). This maximum peak is similarly justified by $\varepsilon_2(\omega)$ in Figure 12(b) at the same pressure. Moreover, the $\varepsilon_1(\omega)$ tends to converge at circa 9 eV and beyond this range progresses parallel to the energy axis. This

behavior reflects the minimum polarization and dispersion of incident photons within this energy range. At zero energy, the calculated static dielectric constants $\varepsilon_1(0)$ within the pressure range lies between 204.78 and 134.63 respectively. The elevated minimal positive values at $\varepsilon_1(0)$ signify critical electrical energy storage ability and degree of polarization in α-AlH_3 hydride (Candan *et al*., 2025). In addition, below zero in the negative regime, $\varepsilon_1(\omega)$ for the different pressures lies in the range 2.15 – 17.61 eV. The negative values satisfy a significant metallic character (Hosen *et al.*, 2025, Gregory *et al*., 2024) of the compound. The relation linking the dielectric function to the electronic band structure (EBS) given as $\left[\varepsilon_1(0) \approx 1 + \left(\hbar\omega_p / E_g\right)^2\right]$, is significant in that higher band gap energy E_g generates minimal $\varepsilon_1(\omega)$ value as prescribed in Penn model (Penn, 1962). Also, the optical spectra of $\varepsilon_1(0)$ can be connected to refractive index by $[n^2(0) = \varepsilon_1(0)]$ (Aliabad & Chahkandi, 2018). The evaluated static refractive index, $n(0)$, lies in the range of 11.25 – 14.29 (from 1 – 8 GPa).

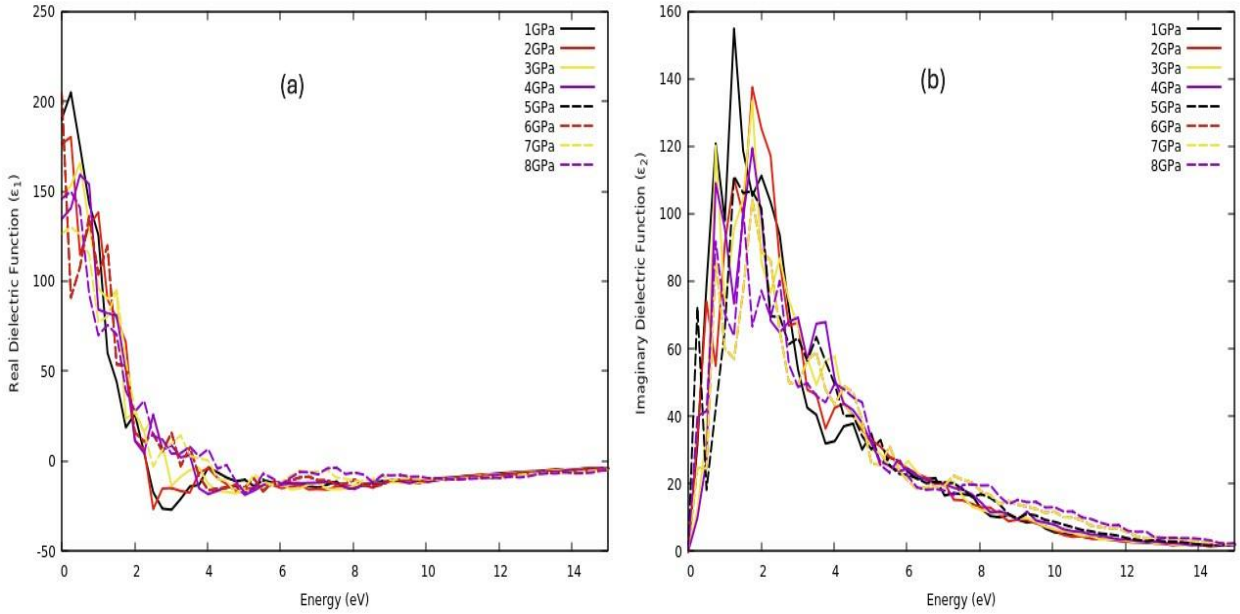

Figure 12: (a) Real part and (b) Imaginary part of dielectric function versus energy at various applied pressures

Figure 12(b) displays the calculated imaginary dielectric function $\varepsilon_2(\omega)$ and shows three prominent peaks each as critical points that represent the thresholds for the optical transitions. These peaks occur between the ranges of energy 0.31 – 2.57 eV along the x-direction, which could be described from the DOS spectra. The prominent peaks appear due to interband electronic transitions leading to the orbital hybridization of the H(1s)-, Al(1s)-, and Al(2p)-states in the compound. The Figure shows that for the applied pressure promising applications are favorable for infrared and visible light technology.

In Figure 13, the electron energy loss (EEL) function at different pressures calculated using Eq. (9) is displayed as a photon energy dependent function. The EEL function shown illustrates the scattering probability of photoelectrons. Observations from Figure 13 show that below 33.00 eV there is no energy loss, indicating the material's ability to retain photoelectrons within this energy range. The highest energy loss value is 78.7 at 36.69 eV. Energy loss drops to zero beyond 44.10 eV. The

highest energy of the EEL function L(ω) is defined as the energy of plasmon volume ($\hbar\omega_p$). The real part of dielectric function $\varepsilon_1(\omega)$ equals zero at plasma resonances. Thus, from Figure 13, the obtained maximum value of $\hbar\omega_p$ for the binary hydride (α-AlH_3) is favored at 3 GPa with a photon energy of 36.69 eV at 78.7 peak maximum. In Figure 13, the outstanding promising sharp peak (with solid-yellow spectra) seen denoting 3 GPa is a deviation showing the highest interband excitations between the HOMO-LUMO transition. Consequently, this abrupt frequency discontinuity of EEL in the optical peaks at 3 GPa is an indication of a rise and sudden drop in spectra function due to the applied pressures, signaling a phase transition point. The above optical observations confirm the low pressure induced phase transition of α-AlH_3 at 3 GPa as observed in Figure 4(a) (electronic property), Figure 5 (structural property), and Figure 6, respectively. Moreso, at energies less than 33 eV the hydride exhibits a promising photo-absorbing property. This photo-absorbing behavior herein showcases trends similar to ZnO_2 (Thapa *et al.*, 2015).

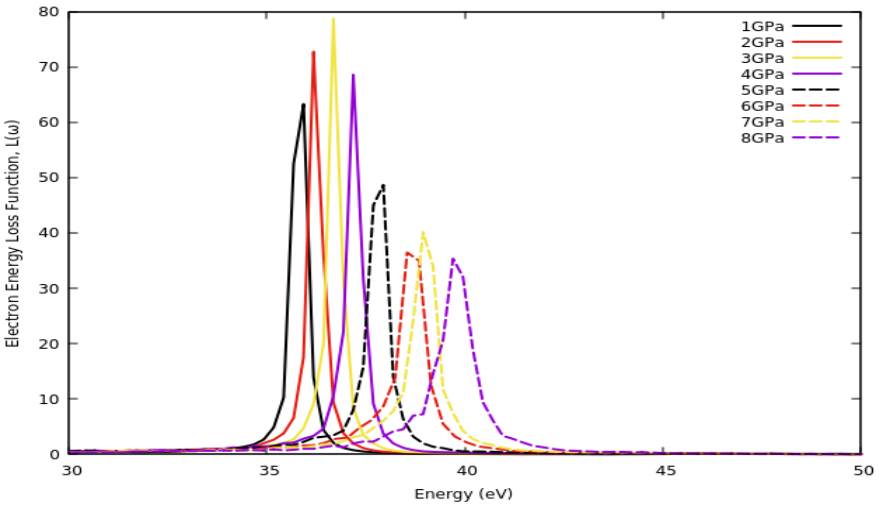

Figure 13: Electron energy loss (EEL) function versus energy at various applied pressure

4.0 Conclusion

In this research, we explored the electronic, structural, thermodynamic, and optical properties of the α-AlH_3 as a promising hydrogen storage material. By optimization of the structure using the generalized gradient approximation (GGA), implemented in the density functional theory (DFT)-based quantum espresso code, we report a gravimetric storage capacity of 10.08% and a desorption temperature value in agreement with the experiments. The electronic and structural analyses reveal that the bulk hydride is a semiconductor with an indirect band gap of 2.16 eV. Also, the total and projected densities of states of α-AlH_3 are calculated to understand the relative energetic contributions of electrons, leading to the hybridization and nature of bonding. From the calculated Al–H bond length, it is found that α-AlH_3 exhibits a covalent bonding nature. Within the limits of the applied pressures, the thermodynamic and optical properties, such as real and imaginary parts of dielectric function, and the electron energy loss function $L(\omega)$ as well as the enthalpy ΔH, free energy, entropy S and heat capacity C_V are calculated. The optical properties calculation of $L(\omega)$ at 3 GPa reasonably confirms the phase transition results computed from both the electronic band structure and the structural analysis. Further confirming this phase transition at 3 GPa is the thermodynamic analysis of the enthalpy ΔH, free energy (− 0.04 Ry), entropy S, and heat capacity. The obtained results predict a phase transition occurring at a pressure of 3 GPa. This suggests that α-AlH_3

may serve as a good energy storage candidate, and also a promising photo-absorber at energies lower than 33 eV.

Acknowledgments:
This article is dedicated to the memory of Professor John O. A. Idiodi (Late), who made significant and valuable contributions to the previous and recent past, leading to the conceptualization of this study.

Conflict of Interest: The authors declare that they have no conflict of interest.

References

Aguayo, A. & Singh, D. J. (2004). Electronic structure of the complex hydride $NaAlH_4$. *Phys. Rev. B* 69, 155103.

Ahmed, B., Tahir, M.B., Li, A. & Sagir, M. (2024). First principles screening of structural, electronic, optical and elastic properties of Cu-based hydrides-perovskites $XCuH_3$ (X= Ca and Sr) for hydrogen storage applications. *Int. J. Hydrogen Energy*, 54, 1001–1007.

Ain, Q., Naeem, H.T., Ali, M., Munir, J., Bibi, Z., Ghaithan, H.M., Ahmed, A.A.A. & Qaid, S.M.H. (2024). A precise prediction of structure stability and hydrogen storage capability of $KCdH_3$ perovskite hydride using density functional theory calculations, *J. Energy Storage*, 100: 113734

Aliabad, H. A. R. & Yalcin, B.G., (2017). Optoelectronic and thermoelectric response of - of band gap from direct to indirect. *J. Mater. Sci.: Mater. Electron.*, https://org.doi/10.1007/s10854-017-7368-6

Aliabad, H.A.R. & Chahkandi, M. (2018). Theoretical study of crystalline network and optoelectronic properties of erlotinib hydrochloride molecule: non-covalent interactions consideration. *Chem. Pap.* 73, 737–746.

Baranowski, B. & Tkacz, M. (1983). The equilibrium between solid aluminium hydride and gaseous hydrogen. *Zeitschrift für Physikalische Chemie,* 135 (135), 27 – 38.

Baranowski, B., Hochheimer, H.D., Strossner, K., Honle, W. (1985). High pressure x-ray investigation of AlH_3 and Al at room temperature. *J. Less-Common Met*., 113, 341–347.

Baroni, S., Giannozzi, P., Isaev, E. (2010). Density-functional perturbation theory for quasi-harmonic calculations, *Rev. Mineral. Geochem*. 71 (1), 39–57.

Becke, A.D., (1988). Density-functional exchange-energy approximation with correct asymptotic behavior. *Phys. Rev. A*. 38 (6): 3098–3100.

Becke, A.D. (2014). Perspective: Fifty years of density-functional theory in chemical physics. *J. Chem. Phys.* 140 (18): A301.

Bencheikh, M. & Farh, L.E. (2024). Modeling and simulation of the structural, and optoelectronic properties of aluminum trihydride (β-AlH_3) for hydrogen storage, *Intl. J. Hydrogen Energy*, 94, 223–231.

Brower, F.M., Matzek, N.E., Reigler, P. F., Rinn, H. W., Roberts, C. B., Schmidt, D. L., Snover, J. A., Terada, K. (1976). "Preparation and properties of aluminum hydride". 98. J. Am. Chem. Soc.: 2450–2454.

Candan, A. & Akbudak, S. (2025). First-principles calculations on the physical properties of Zr-based perovskites $LiZrH_3$ and $KZrH_3$ for potential

hydrogen storage applications, *Intl. J. Hydrogen Energy* 129, 199–210.

Ciezak-Jenkins, J. A. (2011). Low-pressure Structural Modification of Aluminium Hydride. Weapons and Materials Research Directorate, ARL (Army Research Laboratory)., Aberdeen Proving Ground, MD 21005-5069. ARL-TR-5463, 1 – 14.

Drozd, V., Garimella, S., Saxena, S., Chen, J. & Palasyuk, T. (2012). High-Pressure Raman and X-ray Diffraction Study of β- and γ-Polymorphs of Aluminum Hydride. *J. Phys. Chem.* C, 116, 3808 – 3816.

Ekong, S.A, Fuwape, I.A. & Odo, E.A. (2014b). Ab initio study of the electronic structure of silicon quantum dots. *J. Nig. Asso. Math. Phys*., 26, 177 – 186.

Ekong, S.A. & Oyegoke, D.A. (2016). QMC calculations of total energy and bond length of some polyatomic organic molecules, *Intl. Lett. Chem. Phys. Astron.* 64, 63 – 68.

Ekong, S.A., Ebomwonyi, O. & Idiodi, J.O.A. (2014a). Closed-shell ground state energy calculations of the first-row diatomic molecules using quantum Monte Carlo casino - code, *J. Nig. Assoc. Math. Phys.*, 28 (1), 317 – 326.

Ekong, S.A., Oloye, M.T. & Oyegoke, D. A. (2015). Ground-state energy calculation of helium atom using quantum Monte Carlo casino-code, *Adv. Phys. Theo. Appl.* 46 (1): 1 – 6.

Ekwere, E.J., Emah, J.B. & Ekong, S. A. (2024). Structural, Electronic, Thermophysical and Optical Investigation of Tetragonal ($C11_b$ – $CrSi_2$) Material: A Theoretical Analysis, *Res. J. Sci. Techn.*, 4(4): 23 – 38.

Giannozzi, P., Andreussi, O., Brumme, T., Bunau, O., Nardelli, M.B., Calandra, M., Car, R., Cavazzoni,C., Ceresoli, D., Cococcioni, M., Colonna, N., Carnimeo, I., Corso, A. D., Gironcoli, S. de, Delugas, P., DiStasio Jr, R.A., Ferretti, A., Floris, A., Fratesi, G., Fugallo, G., Gebauer, R., Gerstmann, U., Giustino, F., Gorni, T., Jia, J., Kawamura, M., Ko, H-Y., Kokalj, A., Küçükbenli, E., Lazzeri, M., Marsili, M., Marzari, N., Mauri, F., Nguyen, N.L., Nguyen, H-V., Roza, A. O. d-l, Paulatto, L., Poncé, S., Rocca, D., Sabatini, R., Santra, B., Schlipf, M., Seitsonen, A.P., Smogunov, A., Timrov, I., Thonhauser, T., Umari, P., Vast, N., Wu, X., Baroni, S. (2017). Advanced capabilities for materials modelling with QUANTUM ESPRESSO, *J. Phys.: Condens. Matter* 29 (46), 465901.

Giannozzi, P., Baroni, S., Bonini, N., Calandra, M., Car, R., Cavazzoni, C., Ceresoli, D., Chiarotti, G.L., Cococcioni, M., Dabo, I., Dal Corso, A., Fabris, S., Fratesi, G., de Gironcoli, S., Gebauer, R., Gerstmann, U., Gougoussis, C., Kokalj, A., Lazzeri, M., Martin-Samos, L., Marzari, N., Mauri, F., Mazzarello, R., Paolini, S., Pasquarello, A., Paulatto, L., Sbraccia, C., Scandolo, S., Sclauzero, G., Seitsonen, A.P., Smogunov, A., Umari, P. & Wentzcovitch, R. M. (2009). QUANTUM ESPRESSO: a modular and open-source software project for quantum simulations of materials. *J. Phys*.: *Condensed Matter* 21(39), 395502 – 395521.

Goedecker, S., & Teter, M. (1996). Separable dual-space Gaussian pseudopotentials. *Physical Review B - Condensed Matter*

and Materials Physics, *54*(3), 1703–1710.

Goncharenko, I.N., Eremets, M.I., Hanfland, M., Tse, J.S., Amboage, M., Yao, Y. & Trojan, I.A. (2008). Pressure-Induced Hydrogen-Dominant Metallic State in Aluminium Hydride. *Phys. Rev. Lett. (PRL)* 100, 045504: 1 – 4.

Goncharenko, I.N., Glazkov, V.P., Irodova, A.V. & Somenkov, V.A. (1991). Neutron diffraction study of crystal structure and equation of state AlD_3 up to the pressure of 7.2 GPa, *Physica B: Conden. Matt.*, 174, 117 – 120.

Graetz, J. & Reilly, J. J. (2006). Thermodynamics of the α, β and γ polymorphs of AlH_3. *J. Alloys Compd.*, 424, 262 – 265.

Graetz, J., Chaudhuri, S., Lee, Y., Vogt, T., Muckerman, J.T. & Reilly, J.J. (2006). Pressure-induced structural and electronic changes in α-AlH_3. *Phys. Rev. B*, 74, 214114:1 – 214114:7.

Graetz, J., Chaudhuri, S., Wegrzyn, J., Celebi, Y., Johnson, J.R., Zhou, W. & Reilly, J.J. (2007). J. Phys. Chem. C, 111, 19148 – 19152.

Graetz, J., Reilly, J.J., Yartys, V.A., Maehlen J.P., Bulychev, B.M., Antonov, V.E., Tarasov, B.P. & Gabis, I.E. (2011). Aluminum hydride as a hydrogen and energy storage material: Past, present and future. *J. Alloys Comp*. 509S, S517 – S528.

Gregory, E. E., Ekong, S. A. & Emah, J. B. (2024). Ab-initio Assessment of the Electronic, Mechanical, Thermal, Optical and Phonon Properties of B3-AlAs, *Res. J. Sci. Techn.*, 4 (3), 69 – 93.

Grew, K.N., Brownlee, Z.B., Shukla, K.C. & Chu, D. (2012). Assessment of Alane as a hydrogen storage media for portable fuel cell power sources. *J. Power Sources*. 217, 417–430.

Hartwigsen, C., Goedecker, S., & Hutter, J. (1998). Relativistic separable dual-space Gaussian pseudopotentials from H to Rn C. *Physical Review B*, *58*(7), 3641–3662.

Hosen, A., Dahliah, D., Mohammad, N.F.A., Mousa, A.A., & Abu-Jafar, M.S. (2025). A computational study on the comparative analysis of tetragonal complex metal hydride Q2FeH5 (Q = Mg, Ca, Sr) for hydrogen storage applications, Intl. J. Hydrogen Energy, 102, 348 – 359. https://doi.org/-10.1016/j.ijhydene.2025.01.042

Humphries, T. D., Munroe, K. T., Decken, A. & McGrady, G.S. (2013). Lewis base complexes of AlH_3: Prediction of preferred structure and stoichiometry. *RSC: Dalton Transaction*, 42, 6965.

Jolayemi, O. R. & Ekong, S. A. (2020). Electronic, structural, magnetic and mechanical properties of $Mg_{1-x}Sr_xN$ rocksalt from first-principles, *Tran. Nig. Asso. Math. Phys.* 13, 39 – 44.

Karazhanov, S. Z., Ravindran, P., Vajeeston, P., & Ulyashin, A.G. (2007). Hydride electronics, *Phys. Status Solidi* (a) 204 (10) 3538–3544.

Karazhanov, S. Z., Ulyashin, A.G., Ravindran, P., & Vajeeston, P. (2008). Semiconducting hydrides. *EPL* 82, 72006: 1–5.

Ke, X., Kuwabara, A. & Tanaka, I. (2005). Cubic and orthorhombic structures of

aluminum hydride AlH_3 predicted by a first-principles study, *Phys. Rev. B* 71, 184107: 1 – 7.

Kohn, W. & Sham, L.J. (1965). Self-consistent equations including exchange and correlation effects, *Phys. Rev.*, 140 (4A): A1133–A1138.

Malica, C. & Corso. A.D. (2020). Quasi-harmonic temperature dependent elastic constants: applications to silicon, aluminum, and silver. *J. Phys.: Condens. Matt.*, 32 (31), 315902.

Masood, M.K., Chaoui, K., Khan, W., Bahajjaj, A.A.A., Bibi, S., Kanwal, A., Rania, C., Bilal, Y. & Rehman, J. (2025). Unveiling the potential platinum-based hydrides for solid-state hydrogen storage application: A DFT study, *Materi. Sci. Semiconductor Processing*, 188, 15, 109214.

Monkhorst, H.J. & Pack, J.D. (1976). Special points for Brillouin-zone integrations. *Phys. Rev. B*, 13 (12), 5188.

Mouchou, S., Toual, Y., Azouaoui, A., Maouhoubi, A., Masrour, R., Rezzouk, A. (2023). Temperature dependence of thermodynamic and mechanical properties of Fe_2RhSi and Fe_2RhGe: An ab-initio investigation. Solid State Communications 376: 115374.

Mujica, A., Rubio, A., Munoz, A. & Needs, R.J. (2003). High-pressure phases of group-IV, III–V, and II–VI compounds. *Reviews of Modern Physics, 75*, 863–912.

Musari, A. (2021). Electronic, mechanical, vibrational and thermodynamic properties of FeXSb (X= Hf and Nb) Half-Heusler alloys from first-principles approach. *Solid State Sciences*, 122: p. 106755.

Obeidat, A., Alrousan, A. & Abu-Rajou, S. (2025). First-principles study of structural, hydrogen storage, mechanical, electronic, and optical properties of K_2NaXH_6 (X = Al, As, Bi, Ga, In) double perovskite hydrides, *J. Power Sci*., 642: 236944.

Orimo, S., Nakamori, Y., Eliseo, J.R., Züttel, A. & Jensen, C.M. (2007). Complex Hydrides for Hydrogen Storage. *Chem. Rev.,* 107, 4111 – 4132.

Orimo, S., Nakamori, Y., Kato, T., Brown, C. & Jensen, C.M. (2006). Intrinsic and mechanically modified thermal stabilities of α-, β- and γ-aluminum trihydrides AlH_3. *Appl. Phys. A* **83**, 5–8.

Pan, Y. & Yu, E. (2022). New insight into the structural and physical properties of AlH_3, *Intl. J. Energy Research*. https://doi.org/10.1002/er.8534.

Pan, Y. (2024). Exploring the structural, physical properties and hydrogen storage properties of LiBHx (x = 1 and 4) lithium borohydrides. *Ceram. Int*., 50(2), 3837–3842.

Penn, D. R. (1962). Wave-number-dependent dielectric function of semiconductors. *Phys. Rev. B*, 128(5), 2093.

Perdew, J.P., Burke, K. & Ernzerhof, M. (1996), Generalized gradient approximation made Simple, *Phys. Rev. Lett*. 77, 3865.

Rehman, Z.U., Rehman, M.A., Alomar, S.Y., Rehman, B., Awais, M., Amjad, M., Sikiru, S., Ali, E.M. & Hamad, A. (2024). Hydrogen Storage Capacity of Lead-Free Perovskite NaM_TH_3 (M T

=Sc, Ti, V): A DFT Study, *Intl. J. Energy Research*, 4009198: 1–14.

Rehman, Z.U., Rehman, M.A., Rehman, B., Sikiru, S., Qureshi, S., Ali, E.M., Awais, M., Amjad, M., Iqbal, I., Rafique, A. & Bibi, S. (2023). Ab initio insight into the physical properties of $MgXH_3$ (X = Co, Cu, Ni) lead-free perovskite for hydrogen storage application. *Environmental Science and Pollution Research*, 30: 113889–113902.

Ren, L., Zheng, W., Yang, Y., Xu, X., Jiao, P., Cui, J. (2023). DFT Study on Co–H Bond Dissociation Enthalpies of Cobalt Hydrides in Metal-Catalyzed Hydrogen Atom Transfer Reactions, *Russian Journal of Physical Chemistry,* 97 (12): 2755 – 2767.

Savić, M., Radaković, J. & Batalović, K. (2017). Study on electronic properties of α-, β- and γ-AlH_3 – The theoretical approach. *Computational Mater. Sci.,* 134, 100–108.

Shahzad, M.K., Hussain, S., Khan, M.N., Aslam, M.J., Mohammed, R.M., Tirth, V., Alqahtani, H., Algahtani, A., Al-Mughanam, T. & Azeem, W. (2024). Computational insights of double perovskite Na_2CaCdH_6 hydride alloy for hydrogen storage applications: a DFT investigation, *Scientific Reports*, 14:25102.

Sinke, G. C., Walker, L. C., Oetting, F. L. & Stull, D. R. (1967). Thermodynamic properties of aluminum hydride, *J. Chem. Phys*. 47 (8): 2759–2761.

Song, Y. (2013). New perspectives on potential hydrogen storage materials using high pressure. *Phys. Chem. Chem. Phys*., 15, 14524 – 14547.

Takeda, Y., Saitoh, Y., Saitoh, H., Machida, A., Aoki, K., Yamagami, H., Muro, T., Kato, Y. & Kinoshita, T. (2011). Electronic structure of aluminum trihydride studied using soft X-ray emission and absorption spectroscopy. *Phys. Rev*. B, 84, 153102: 1 – 4.

Tatsumi, K., Muto, S., Ikeda, K. & Orimo, S. (2012). Chemical Bonding of AlH_3 Hydride by Al-L2,3 Electron Energy-Loss Spectra and First-Principles Calculations, *Materials*, 5, 566-574

Thapa, R., Ghosh, S., Sinthika, S., Kumar, E.M., Park, N. (2015). Magnetic, elastic and optical properties of zinc peroxide (ZnO_2): First principles study. *Journal of Alloys and Compounds*, 620, 156–163.

Tkacz, M., Filipek, S. & Baranowski, B. (1983). High-pressure synthesis of aluminum-hydride from the elements, *Pol. J. Chem*., 57, 651 – 653.

Tkacz, M., Palasyuk, T., Graetz, J. & Saxena, S. (2008). High-pressure Raman spectroscopy study of α and γ polymorphs of AlH_3. *J. Raman Spectroscopy*, 39, 922 – 927.

Tufail, D., Ahmed, U., Haleem, M., Amin, B. & Shafiq, M. (2025). DFT study of alkaline earth metals $NaXH_3$ (X = Be, Mg, Ca, Sr) for hydrogen storage capacity, *RSC Adv.,* 15, 337–347.

Turley, J.W. & Rinn, H.W. (1969). The crystal structure of aluminum hydride. *Inor. Chem.* **8** (1): 18–22.

Usman, M., Wu, A., Bibi, N., Rehman, S., Rehman, M.A., Ahmad, S., Rehman, H.U., Ashraf, M.U., Rehman, Z.U. & Altaf, M. (2024). Hydrogen storage application of Zn-based hydride -

perovskites: a computational insight, *Optical and Quantum Electronics*, 56, 1478: 1–17.

Vajeeston P., Ravindran P. & Fjellvåg H. (2008). Novel high pressure phases of β-AlH_3: A density-functional study, *Chem. Mater.*, 20 (19), 5997 – 6002.

Vajeeston P., Ravindran P. & Fjellvåg H. (2011). Stability enhancement by particle size reduction in AlH_3. J. Alloy. Compd. https://org.doi.10.1016/j.jallcom.2010.11.110

Van Setten, M.J., Popa, V.A., de Wijs, G.A. & Brocks, G. (2007). Electronic structure and optical properties of lightweight metal hydrides, *Phys. Rev. B*, 75, 035204.

Wang, Y., Yan, J.-A. & Chou, M.Y. (2008). Electronic and vibrational properties of γ-AlH_3. *Phys. Rev. B,* 77(1), 014101: 1–8.

Yu, C.-F., Liu, Y.-L., (2025). DFT Study of Au3In and Au3In2 Intermetallic Compounds: Structural Stability, Fracture Toughness, Anisotropic Elasticity, and Thermophysical Properties for Advanced Applications. *Materials*, 18, 1561. https://doi.org-/10.3390/ma18071561